Check for updates

A floating 5 μm-diameter needle electrode on the tissue for damage-reduced chronic neuronal recording in mice†

Koji Yamashita,[a] Hirohito Sawahata,[b] Shota Yamagiwa,[a] Shohei Yokoyama,[c] Rika Numano,[de] Kowa Koida[df] and Takeshi Kawano (ID) *[a]

Microelectrode technology is essential in electrophysiology and has made contributions to neuroscience as well as to medical applications. However, it is necessary to minimize tissue damage associated with needle-like electrode on the brain tissue and the implantation surgery, which makes stable chronic recording impossible. Here, we report on an approach for using a 5 μm-diameter needle electrode, which enables the following of tissue motions, *via* a surgical method. The electrode is placed on the brain tissue of a mouse with a dissolvable material, reducing the physical stress to the tissue; this is followed by the implantation of the electrode device in the brain without fixing it to the cranium, achieving a floating electrode architecture on the tissue. The electrode shows stable recording with no significant degradation of the signal-to-noise ratios for 6 months, and minimized tissue damage is confirmed compared to that when using a cranium-fixed electrode with the same needle geometry.

Introduction

Electrophysiology with microelectrode technology is an essential method in neuroscience, making contributions to the understanding of the nervous system and to medical applications. Extracellular signals with high spatiotemporal resolution can be recorded using a needle electrode penetrating into the tissue, such as a multichannel-electrode array to record multiple neurons[1–4] or a flexible electrode to minimize the mechanical mismatch between the needle (electrode) and the soft tissue (brain).[5–10] For long-term neuronal recording, it is necessary to minimize tissue responses, including neuronal death due to electrode penetration, and avoid the decrease in recording stability, including the signal-to-noise ratio (SNR) during device implantation. However, typical methods that employ these

[a] Department of Electrical and Electronic Information Engineering, Toyohashi University of Technology, Aichi, Japan. E-mail: kawano@ee.tut.ac.jp
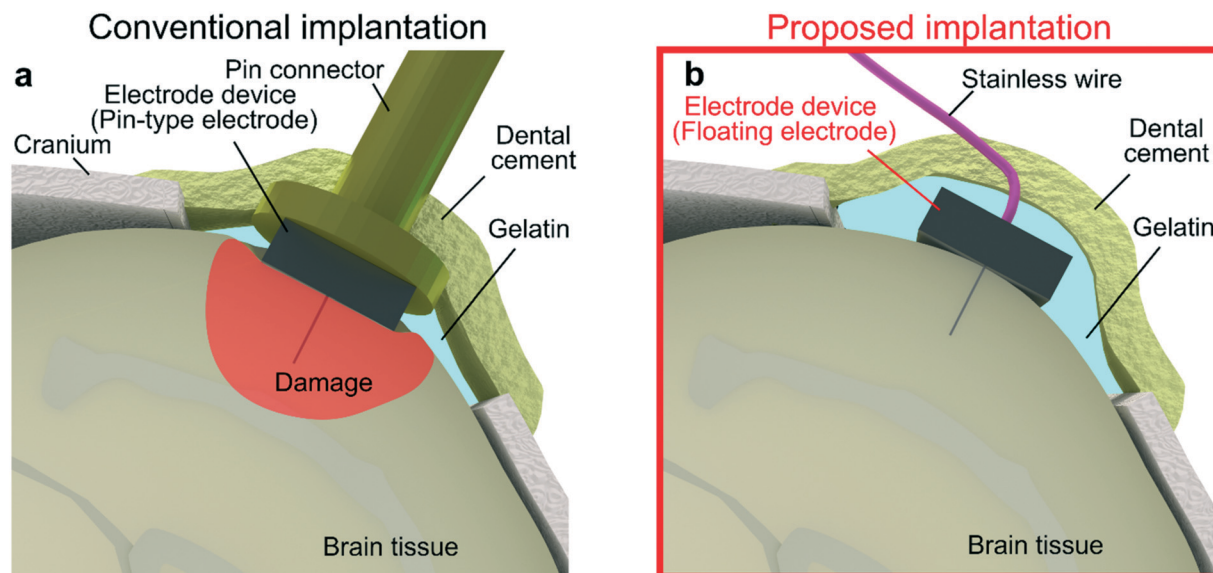*[b] National Institute of Technology, Ibaraki College, Ibaraki, Japan*
[c] TechnoPro, Inc., TechnoPro R&D, Company, Tokyo, Japan
[d] Electronics-Interdisciplinary Research Institute (EIIRIS), Toyohashi University of Technology, Aichi, Japan
[e] Department of Applied Chemistry and Life Science, Toyohashi University of Technology, Aichi, Japan
[f] Department of Computer Science and Engineering, Toyohashi University of Technology, Aichi, Japan
† Electronic supplementary information (ESI) available. See DOI: 10.1039/d1lc01031j

invasive needle electrodes with a diameter of more than 10 μm cause significant damage to the brain tissue,[11–14] making stable recording impossible.[15,16]

Recent advances in microelectromechanical system technology enable us to fabricate extracellular needle electrodes with a diameter of less than 10 μm (*e.g.*, <3 μm (ref. 17 and 18) for *in vitro* recording and 8.6 μm,[19] 5 μm,[20,21] and 300 nm (ref. 22) for *in vivo* recording), thereby minimizing tissue response. In addition, in chronic applications, the physical stress at the interface between the device substrate [*e.g.*, silicon (Si)] and tissue surface induces sustained inflammation and tissue response. In particular, a large geometry of the device substrate increases areas of craniotomy and tissue damage. The approach reported in this study involves using an electrode device that has a 5 μm-diameter needle electrode on a $1 \times 1 \times 0.5$ mm^3 substrate; in addition, a surgical procedure for the chronic device implantation is proposed. Because of brain tissue pulsation, conventional implantations, in which the electrode is fixed to the cranium, cause significant chronic inflammation[20] (Fig. 1a). To avoid these difficulties, a floating architecture for implantable devices, such as Smart dust on the tissue (nerve or muscle),[23,24] can be offered. By utilizing the surgical technique, the electrode device is implanted in the brain without being fixed to the cranium, resulting in a floating 5 μm-diameter needle electrode on the tissue to follow the pulsations (Fig. 1b). For physical stress reduction in the tissue during the electrode penetration, the device is attached to a

Fig. 1 Comparison of electrode implantation. a) Schematic showing the conventional implantation, in which the electrode is fixed to the cranium of the brain. b) Schematic showing the proposed implantation, in which the electrode packaged with a flexible lead is implanted in the brain without fixing to the cranium, achieving a "floating electrode" architecture on the tissue.

manipulator with a material that dissolves. We demonstrated the device implantation in mice and chronic experiments while evaluating the signal quality and tissue damage.

Experimental
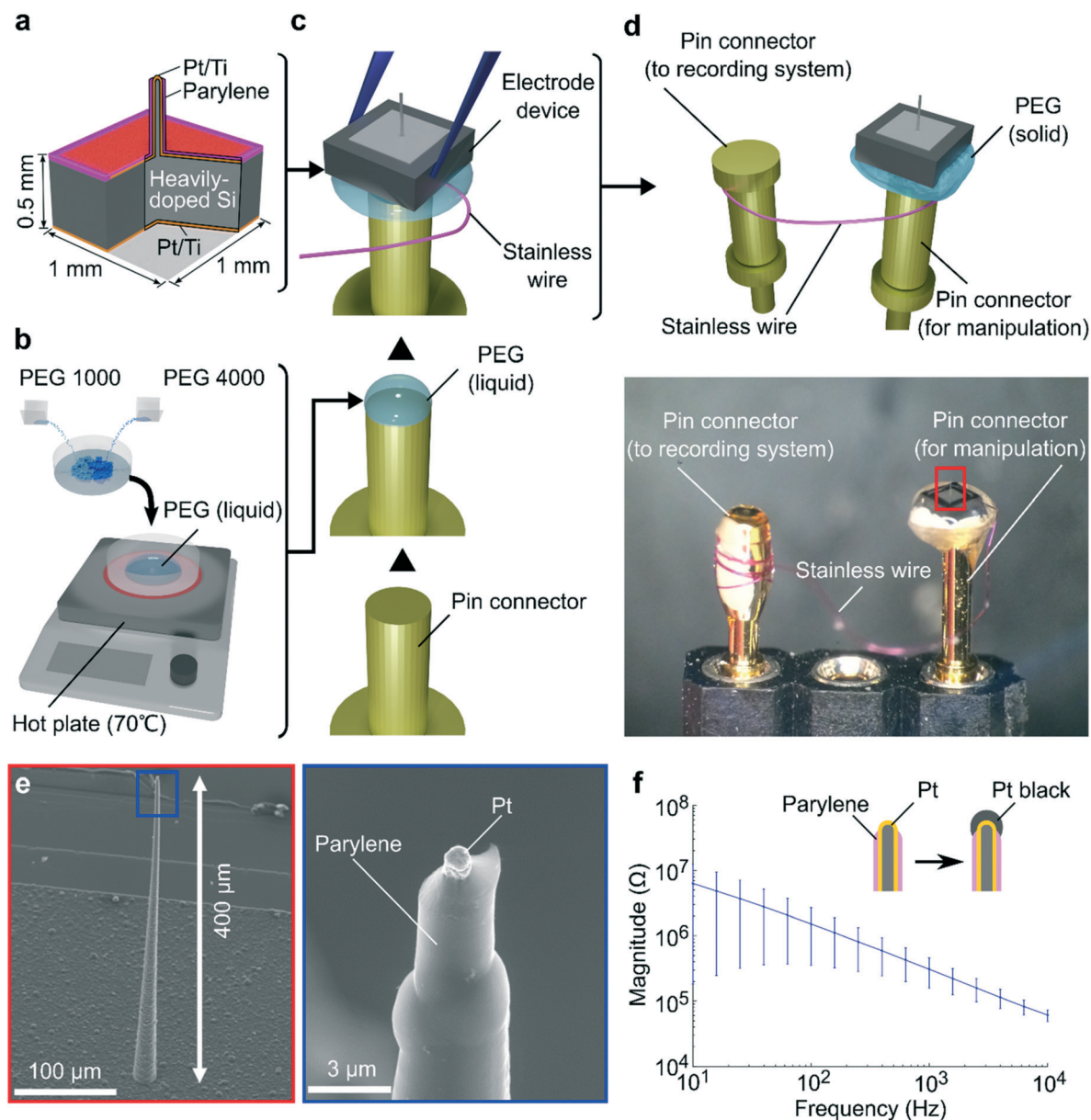
Microneedle electrode device

We used a device that has a 5 μm-diameter 400 μm-length microneedle electrode at the center of a 1 × 1 mm^2 Si substrate [n-type (111)-Si, resistivity = <0.02 Ω cm, thickness = 525 μm][20,25] (Fig. 2a). We used a Si growth technology [gold (Au)-catalyzed vapor–liquid–solid growth of Si (ref. 26)] to fabricate the Si microneedle, which was then metalized with platinum (Pt) and titanium (Ti) (total Pt/Ti thickness = 200 nm) followed by device encapsulation with a biocompatible parylene-C insulator (1 μm in thickness, with the exception of the tip by a plasma process).[20] To achieve the proposed floating electrode, the fabricated electrode device was packaged with an output lead (polyurethane-coated flexible stainless-steel wire; 30 μm in diameter). For device manipulation, the packaged electrode device in our prior work was mounted on a pin-type Au connector using a paraffin wax, which plays a role in device detachment.[27] However, this material should be heated for melting (~70 °C for device detachment). To avoid heating, we used polyethylene glycol (PEG) [two types of PEGs with different melting characteristics were mixed, PEG 1000 : PEG 4000 = 1 : 1 (165-09085 for PEG 1000 and 162-09115 for PEG 4000, FUJIFILM Wako Pure Chemical Corporation, Japan)], which dissolves in liquid (e.g., saline) at room temperature. Fig. 2b and c show the device package with the PEG paste. These two types of PEGs are spread on a dish and then heated (70 °C), to mix as the liquid phase. The PEG paste is

then applied to the tip of a pin connector, and the fabricated electrode device with the stainless wire is assembled. The PEG solidifies at room temperature and is ready for use in animal experimentation. Fig. 2d illustrates the electrode device packaged with the PEG paste, equipped with a stainless wire for the recording ["Pin connector (to recording system)" in Fig. 2d]. Fig. 2e shows the SEM images of the overall and tip section of the fabricated microneedle electrode. The tip and bottom diameters of the microneedle were 1 and 10 μm, respectively.

Owing to the small geometry of the recording site of Pt, the microneedle electrode showed impedance magnitudes ranging from 290 ± 220 MΩ to 580 ± 38 kΩ at 10 Hz to 10 kHz [5.0 ± 0.8 MΩ (mean ± SD) at 1 kHz] in phosphate-buffered saline (PBS) at room temperature. To reduce the electrode impedance, the microneedle tip was modified with a low impedance Pt black material,[28] resulting in the impedance magnitudes that ranged from 6.3 ± 6.1 MΩ to 60 ± 12 kΩ [300 ± 150 kΩ (mean ± SD) at 1 kHz][20,21] (Fig. 2f).

In vivo experiments

For the in vivo experiments, mice (wild-type C57 BL/6 mice, 20–30 g in weight) were anesthetized with isoflurane. After the head of a mouse was fixed with a stereotaxic apparatus (SR-50, Narishige, Tokyo, Japan), parts of the cranium were removed [primary visual cortex (V1), 2.5 mm on the lateral side and 4.0 mm on the caudal side to the bregma, having a diameter of 1–3 mm]. The floating electrode device was attached to a micromanipulator (MO-10, Narishige) to control needle penetration as well as the device placement. The recording site was stereotaxically defined, after which the microneedle penetrated the mouse's brain. After the device

Fig. 2 An electrode device. a) Schematic of the electrode device (1 × 1 mm² surface area, 500 μm thickness), containing a needle electrode with a diameter of 5 μm and a length of 400 μm in the center. b) PEG is prepared for the device package. c) Assembly of the electrode device on a pin connector *via* the PEG paste. d) Schematic and photograph of the packaged electrode device with an output lead (stainless-steel wire). e) SEM images of the overall needle and the needle tip portion. f) Impedance characteristics of Pt black plated microelectrodes measured at room temperature in PBS.

placement, the device was covered with a gelatin sponge, followed by covering with dental cement. All experimental procedures were approved by the Committee for the Use of Animals at Toyohashi University of Technology, and all animal care followed the Standards Related to the Care and Management of Experimental Animals (Notification No. 6, March 27, 1980 of the Prime Minister's Office of Japan).

In visual response recording, the mouse was sedated by intraperitoneal injection of chlorprothixene (100 μl of 0.5% solution per 10 g body weight). For the visual stimulation of the mouse, the mouse was illuminated with a white light-emitting diode (LED) in a dark room. The LED was set to illuminate for 0.5 s at a 3 s interval. The LED was driven by a processing system (RZ2, Tucker-Davis Technologies, Alachua, USA). The timing pulse signals of these stimulations were synchronized to acquire neuronal signals.

In the signal acquisition and processing procedure, the signals recorded from the microneedle electrode were differentially amplified (ZC64, Tucker-Davis Technologies, 1 × 10¹⁴ Ω input impedance) with filters (0.35 Hz for low cutoff and 7.5 kHz for high cutoff). Following signal amplification, the signals were routed to a preamplifier/digitizer (PZ2, Tucker-Davis Technologies) and a digital signal processing

module (RZ2, Tucker-Davis Technologies, Alachua, USA). All digital data were then stored on a hard disk in a Windows PC with a sampling frequency of 25 kHz.

Immunohistochemistry

Six mice (wild-type C57 BL/6, 20–30 g in weight before implantation) were used for the implantation of the floating and pin-type electrodes, respectively. Each electrode was implanted at the V1 of each mouse's right hemisphere. 2 weeks after the electrode implantation, these mice were anesthetized by intraperitoneal injection of urethane (200 μl of 10% solution per 10 g body weight) and then perfusion fixed with 4% paraformaldehyde. Four slice samples (coronal section) from each mouse were prepared. The sections were labeled with GFAP (astrocytes), Iba-1 (microglia), and DAPI (nuclei). Photographs were taken with an Olympus DP74

camera powered by CellSens Dimension software (version 2.2). The intensities of each cell types were based on the outline of each cell generated by edge detection (Find Edges of software ImageJ).

Results

Fig. 3 shows the proposed surgical procedure for the electrode placement on the mouse's brain tissue and the device detachment by using a dissolvable PEG material. The needle electrode penetrated the brain tissue by manipulating the pin connector with a manipulator (Fig. 3a1). By dropping solution (PBS) on the PEG, the solid-phase PEG dissolves (Fig. 3a2). After the PEG is completely dissolved, the electrode's substrate can be detached from the pin connector, and the electrode device remains on the surface of the brain tissue (Fig. 3a3). The time required for the experimental
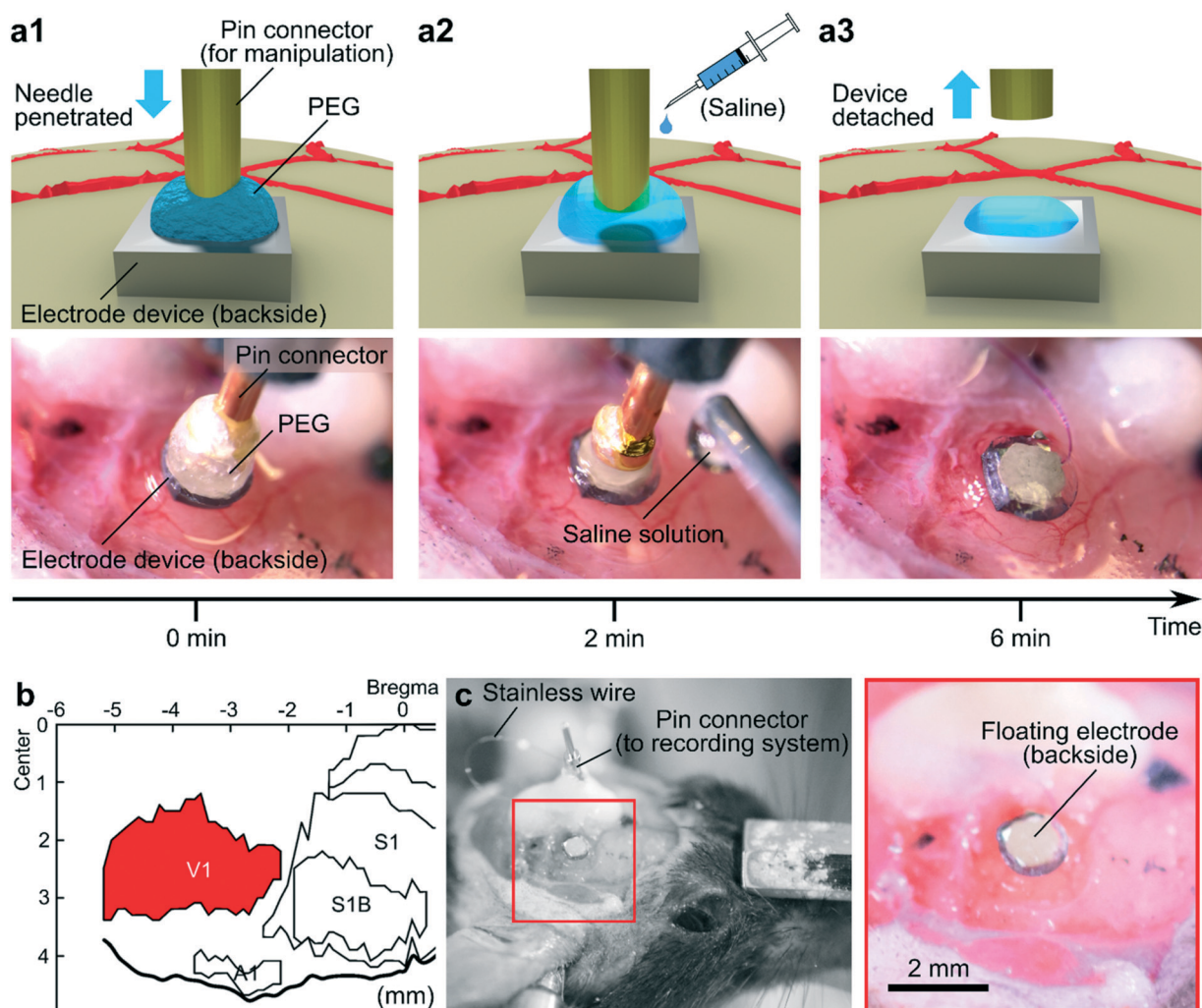
Fig. 3 Placement of the floating electrode on the brain tissue of a mouse. a) Schematic and photograph of each step in the surgical procedure for the electrode penetration: a1) the needle electrode penetrates the brain tissue of the mouse by manipulating the pin connector; a2) dropping PBS to the PEG for detaching the electrode's substrate from the pin connector; and a3) pulling the pin connector upward leaving the electrode device on the tissue. b) Schematic showing the area of the device placement in the cortex (visual cortex, V1). c) Photographs of the electrode device after the surgical method.

procedure was within 6 min (Movie S1†). Fig. 3b and c show an electrode device, which was placed on the V1 on the right hemisphere (2.5 mm on the lateral side and 4.0 mm on the caudal side to the bregma, having a diameter of 1–3 mm). After the device placement, the device was covered with a gelatin sponge and dental cement for chronic recording (see "*In vivo* experiments") (Fig. 4a and b).

We assessed the chronic recording from mice implanted with pin-type and floating electrodes (wild-type C57 BL/6, 20–30 g prior to implantation). Fig. 4c1 and c2 show low-frequency (filtering = 10–80 Hz) and high-frequency (filtering = 500–1000 Hz) band waveforms, respectively, recorded one day after the pin-type electrode was implanted. Fig. 4c3 and c4 show the raster plot diagram and the
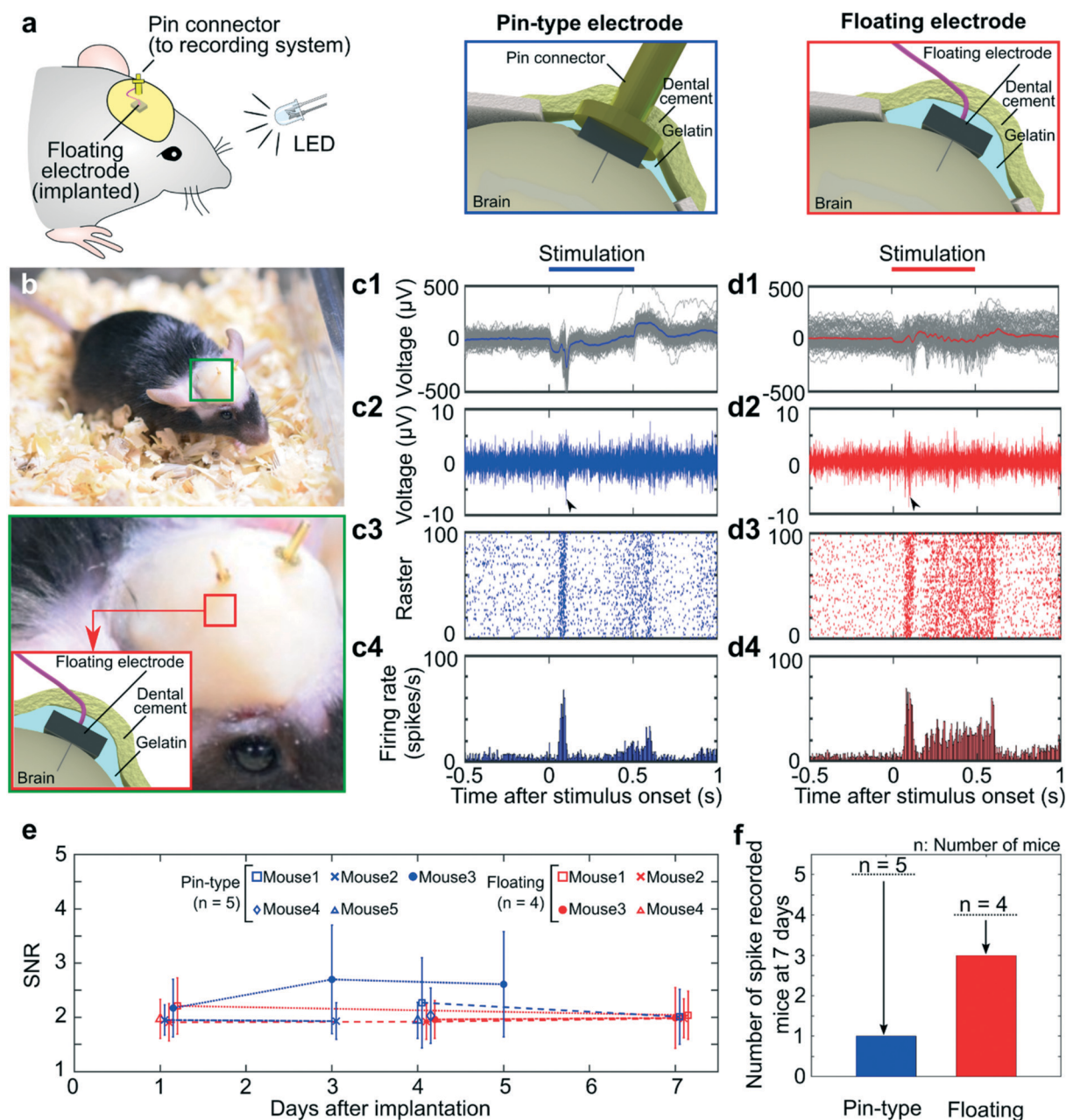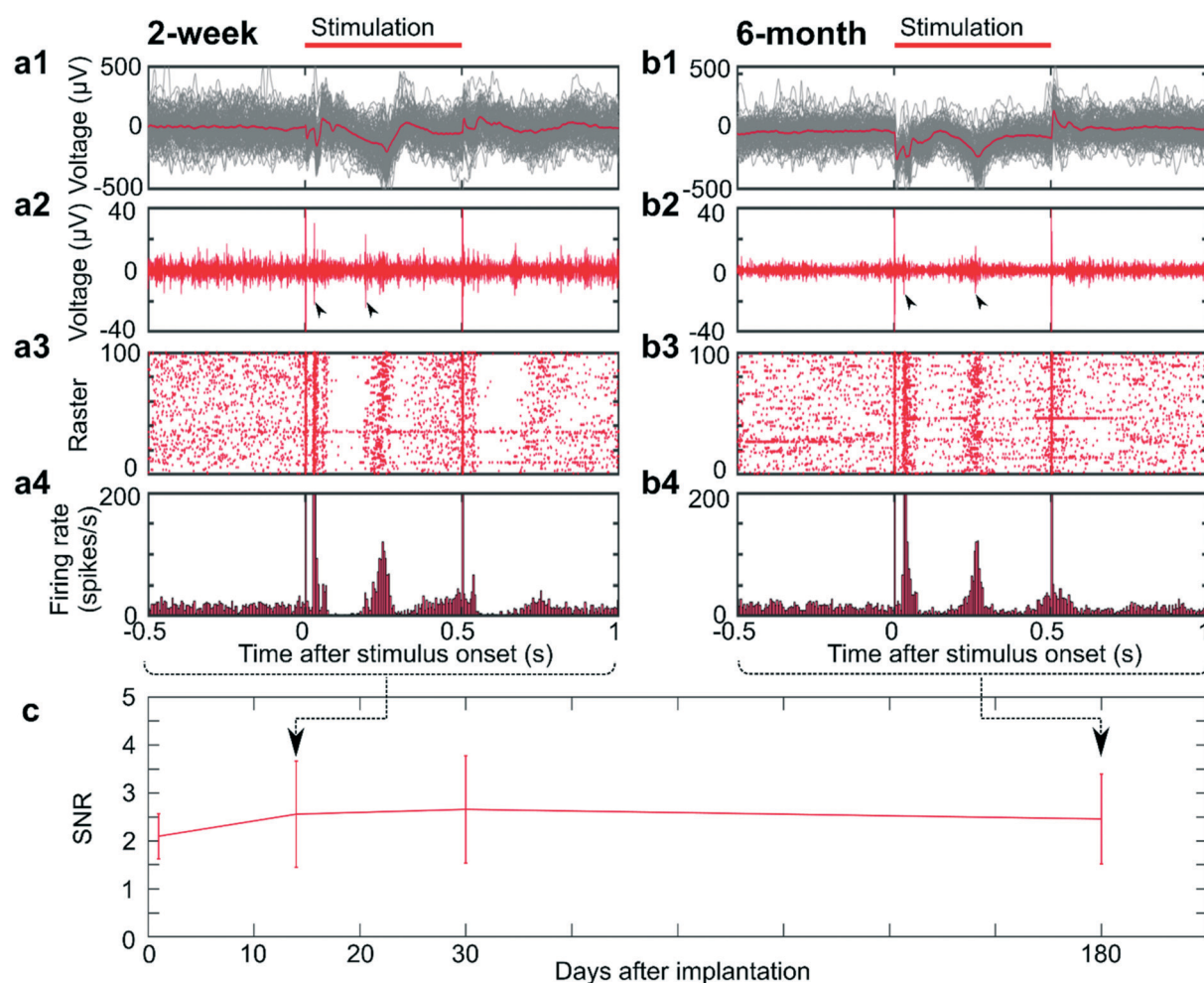

Fig. 4 Chronic *in vivo* neuronal recording for 7 days. a) Schematic of the recording with visual stimulation provided by a light-emitting diode (LED). b) Photographs of a mouse implanted with a floating electrode. To record the visual responses, each device is implanted into the mouse's visual cortex (V1). c1–4) Waveforms recorded from the pin-type electrode 1 day after implantation; c1) an average waveform of low-frequency band signals (filtering = 10–80 Hz, n = 100 trials), c2) a single high-frequency band signal from a single trial (filtering = 500–1000 Hz), and c3, 4) raster plot diagram and PSTH extracted from the high-frequency band signals, respectively (n = 100 trials). The detection threshold was set to 3 × the SD (σ) of the mean signal −0.5 to −1.0 s before the stimulus onset. d1–4) Waveforms recorded from the floating electrode 1 day after implantation. e) SNR of the spikes detected on each electrode implanted mouse for 7 days (mean ± SD, n = 100 trials for each electrode during the recording period). f) Numbers of electrodes detecting spikes from each mouse 7 days after implantation.

peristimulus time histogram (PSTH), respectively, obtained from the high-frequency band signals, with an amplitude threshold of three standard deviations (SDs, σ) of the mean signal −0.5 to −1.0 s before the stimulus onset. Similar to the results obtained with the pin-type electrode, Fig. 4d1 and d2 depict the waveforms from the low and high-frequency bands, respectively, recorded one day after the floating electrode was implanted. Additionally, Fig. 4d3 and d4 show raster plot diagram and the PSTH detected from the high-frequency band signals using an amplitude threshold (3σ of the mean signal, −0.5 to −1.0 s before the stimulus onset). The signals responding to the visual stimuli appeared at approximately 50 ms, for both pin-type and floating electrodes, which was consistent with the latency of mouse's visual response.[29] These results suggest that the recorded signals were the local field potentials (Fig. 4c1 and d1) and the spikes (Fig. 4c2–c4 and d2–d4), which were evoked by the visual stimuli.

Additionally, we evaluated the chronic recording by comparing the signal-to-noise ratio (SNR) of the spikes for a period of 7 days (n = 5 mice for the pin-type electrode and n = 4 mice for the floating electrode, Fig. 4e). The SNR was defined as the peak-to-peak amplitude of the mean waveform 0.005 to 0.1 s after the stimulus onset divided by the 3σ of the noise level. These SNRs are greater than 1.9 (mean) across all electrode types. The duration of the continuous recording, on the other hand, depended not only on the mouse, but also on the type of the implanted electrode. The pin-type electrode demonstrated a decrease in the number of electrodes detecting spike signals (3σ of the mean signal −0.5 to −1.0 s before the stimulus onset) from 5 to 1 on day 7. On the other hand, the floating electrode demonstrated a decrease in the number of electrodes from 4 to 3, indicating that it is more stable than the pin-type electrode (Fig. 4f).

We examined the chronic recording from the floating electrode implanted mouse for a longer period of 6 months

Fig. 5 Chronic *in vivo* neuronal recording with the floating electrode for 6 months. a1–4) Waveforms recorded from the freely moving mouse 2 weeks after the implantation. Top panel represents the timing of the optical stimulation: a1) average waveform of low-frequency band signals (filtering = 10–80 Hz, n = 100 trials), a2) a high-frequency band signal from a single trial (filtering = 500–1000 Hz), and a3, 4) raster plot diagram and PSTH taken from the high-frequency signals (n = 100 trials). The detection threshold was 3 × the SD (σ) of the mean signal −0.5 to −1.0 s before the stimulus onset. b1–4) Waveforms recorded from the free-moving mouse 6 months after the implantation. c) SNR of the spikes detected on the electrode implanted mouse for 180 days (6 months) (mean ± SD, n = 100 trials for each recording period).

(n = 1 mouse, wild-type C57 BL/6, female, 27.8 g in weight before implantation). Fig. 5a1, 2 and b1, 2 show the low-frequency band (filtering = 10–80 Hz) and high-frequency band (filtering = 500–1000 Hz) waveforms for periods of 2 weeks and 6 months, respectively, recorded from the same electrode implanted mouse. Large spikes appeared at 0 and 0.5 s are stimulation-induced artifacts which represent the timing of LED illumination. Fig. 5a3, 4 and b3, 4 also show
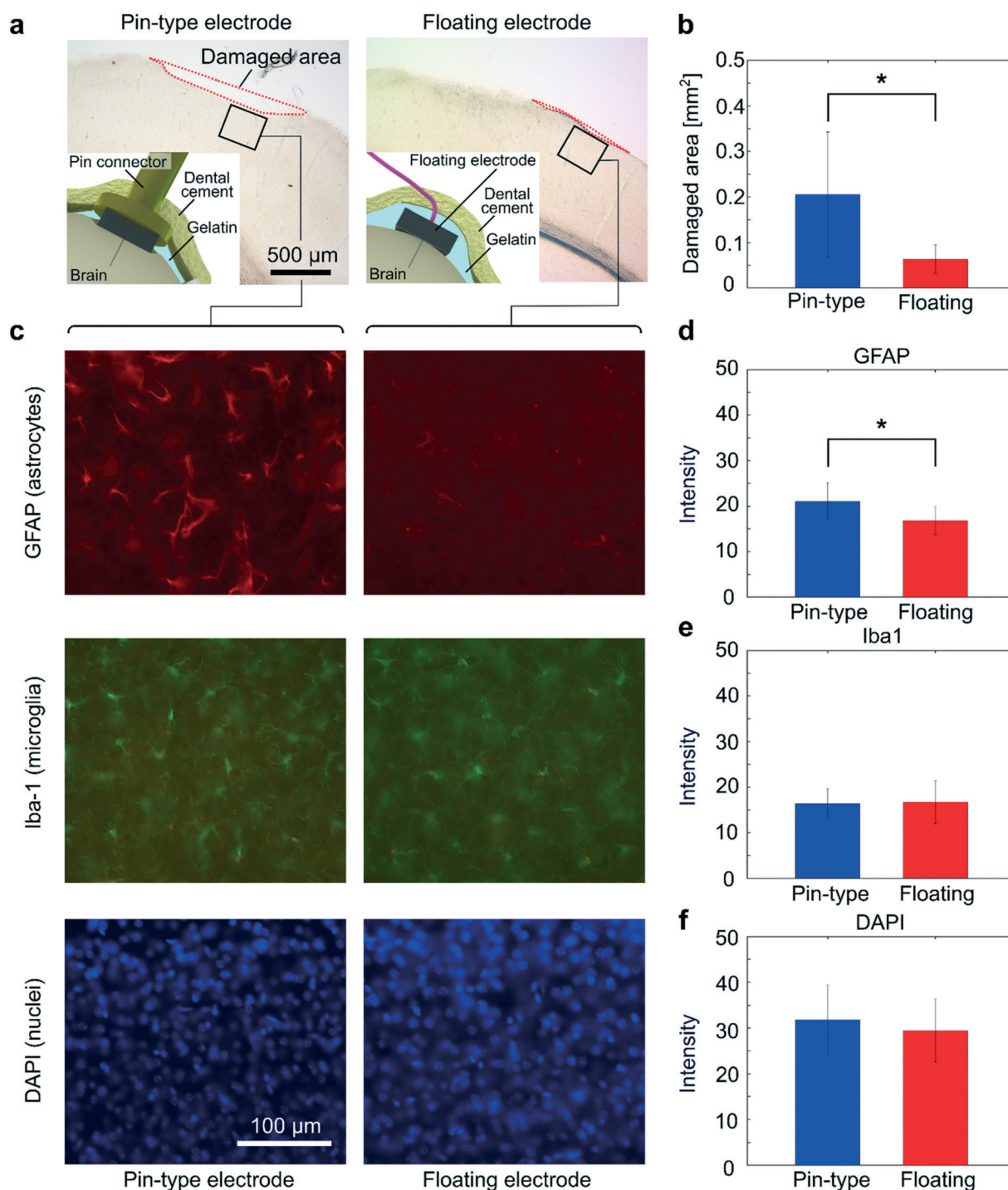
Fig. 6 Histological comparison of the tissue response to chronically implanted conventional pin-type and floating electrodes. a) Photograph of the brain tissues two weeks after the pin-type electrode and floating electrode were implanted. b) Quantitative comparison of the damaged areas using the pin-type and floating electrodes. c) Tissue responses in the visual cortex following 2 week implantation of the pin-type electrode (left panels) and the floating electrode (right panels). The tissues are labelled for reactive astrocytes (GFAP), microglia (Iba-1), and nuclei (DAPI). d–f) Quantitative comparisons of each cell type between the pin-type and floating electrodes using fluorescence intensity in an area of 0.1 mm^2, taken from 24 slice samples of six mice (mean ± SD) (*p < 0.01, t-test).

the raster plot diagrams and the PSTHs of the high-frequency band signals detected at these recording periods (3σ of the mean signal −0.5 to −1.0 s before the stimulus onset). We also analysed the SNR during the recording period (6 months, Fig. 5c), showing a mean SNR of >2.4 from 2 weeks to 6 months without significant degradation.

Additionally, we examined the tissue damage associated with the implanted floating device; we also examined the tissue damage associated with the pin-type electrode (cranium-fixed electrode) using different mice (n = 3 mice for the floating electrode and n = 3 mice for the pin-type electrode).

Fig. 6a shows the brain tissues (coronal section) two weeks after the pin-type electrode and floating device were implanted. Each slice sample shows a dimple-like damaged area at the location of each electrode. Fig. 6b shows a quantitative comparison of these damaged areas, which were calculated by smoothening each tissue surface (the "damaged area" is marked in Fig. 6a with a red dashed line). The floating electrode significantly reduced the damage area compared to the pin-type electrode (24-slice samples from six mice, t-test, *$p < 0.01$).

Fig. 6c shows the histological outcome (coronal brain section) from the V1 of mice 2 weeks after device implantation, including the distribution of labeled reactive astrocytes (GFAP), microglia (Iba-1), and cell nuclei (DAPI) (24-slice samples from six mice, t-test, *$p < 0.01$). In comparison to the pin-type electrode, the floating device exhibits fewer reactive astrocytes (Fig. 6d). The microglia (Iba-1) and cell nuclei (DAPI) associated with the floating electrode were compared to those associated with the pin-type electrode (Fig. 6e and f), and no statistically significant difference was observed. These histological findings indicate that the floating device is capable of recording for extended periods of time while minimizing tissue responses, compared to the pin-type electrode.

Discussion

We proposed the penetration of a microelectrode into the brain tissue and the device detachment with a dissolvable PEG material. The advantage of the proposed surgical procedure is the reduction of physical stress to the tissue during the placement of the device as well as its detachment from the manipulator.[10] Other material such as paraffin wax was also used in our prior work;[27] however, this material needed to be heated for melting (~70 °C), while the used PEG dissolves with PBS at room temperature. The time required for the device placement was ~10 min, a period that can be adjusted by changing the molecular weight of the PEG used. As an advanced way to use the dissolvable material, we can use a PEG-containing bioactive agent, which would reduce the immune responses of the tissue.[30]

For a period of 7 days following implantation, neuronal recording was demonstrated using the pin-type and the proposed floating electrodes implanted in mice. Throughout the recording period, the number of pin-type electrodes detecting spike signals decreased from 5 to 1, while the number of floating electrodes decreased from 4 to 3 (Fig. 4f). The SNR varied between recordings (date and mouse), indicating that there was no significant difference between these two types of electrodes, whereas the recording duration (days) was dependent on the mice. Additionally, we confirmed that some mice did not exhibit spike recording in the early days (1–3 days post implantation); however, these mice displayed spike recording in later days (*e.g.*, 3–7 days post implantation). The temporal loss of spike signals was almost certainly caused by the initial impact of the needle penetration, which compresses and slashes tissue, as well as early responses (*e.g.*, activated microglia[13]). This indicates that the initial impact is independent of the electrode type (pin-type and floating). Additionally, the result of recovered spike recording with the floating electrode in the later days (*e.g.*, 3–7 days post implantation) indicates that the floating electrode contributes to the reduction of inflammation caused by micromotion[31,32] between the electrode and the brain tissue.

We also analyzed the SNR for the floating electrode implanted mouse for 6 months. As known, the implanted device fixed to the cranium induces the motion of the needle on the tissue, resulting in continuous repeated injury to the brain tissue.[11,33,34] This continuous injury forms glial scars, which act as an electrical insulating layer around the recording site of the needle electrode. However, the SNRs measured from 2 weeks to 6 months showed no significant degradation. These results suggest that the floating electrode enables the following of the tissue motion and reduces continuous injury.

We examined the tissue damage associated with the proposed floating electrode and the pin-type electrode. The result indicated that the floating device shows a dimple-like damaged area four times smaller than the damaged area of the pin-type electrode. This result suggested that the device substrate of the pin-type electrode, which is fixed to the cranium, induced pressure to the brain surface during the device implantation. It is known that pressure to the brain tissue causes cerebral ischemia, which results in a blood–brain barrier breach as well as biological inflammation.[35,36] Alternatively, the floating electrode showed a smaller damaged area in the tissue (Fig. 6a and b), which could minimize the issues associated with the electrode implantation.

For the further quantitative comparison of reactive astrocytes (GFAP, Fig. 6d), we confirmed fewer astrocytes with the floating electrode. This result shows the effect of the floating electrode, which was not fixed to the cranium to enable following the tissue. However, comparisons of other cell types, namely, microglia (Iba-1, Fig. 6e) and nuclei (DAPI, Fig. 6f), showed no significant differences between the floating and pin-type electrodes. These phenomena were due to the observation period of 2 weeks, in which microglia

formed in response to the injury (over hours and days[34]) and astrocytes became activated afterwards (for 2 weeks and beyond[13]). Although the floating electrode showed less tissue damage than the pin-type electrode, further minimized tissue damage will be required for future implantation.

For the recording of neuronal activities from the mouse's cortex, we used a single-channel electrode with a 5 μm-diameter microneedle and a device size of $1 \times 1 \text{ mm}^2$ to record the neuronal activity from the mouse cortex. While the floating technique minimized the tissue damage (Fig. 6), the device's dimensions are insufficient for the application of multisite recording with these devices. By arranging these electrode devices, however, a craniotomy area larger than that of a single-channel electrode (>1–3 mm diameter, Fig. 3c) will be required. This indicates that the size of these arranged devices is not small enough for particular brain areas in the mouse (*e.g.*, $2 \times 3 \text{ mm}^2$ in primary visual cortex [V1]). Therefore, we are currently working on fabricating even smaller devices ($<1 \times 1 \text{ mm}^2$) using the same fabrication process used in this work.[20] The results of device miniaturization and multisite recording will be reported in a future publication.

In addition, the floating electrode device presented here includes an additional cable that connects the mouse (electrode device) to the first-stage amplifier of the recording system. Using this cable may result in inhibition of the mouse's behavior as well as a decrease in the recording signal quality due to external noise coupled with the cable. These concerns can be resolved with a wireless electrode recording system.[37–41]

Conclusions

In summary, we proposed a method for chronic neuronal recording in mice in which a 5 μm-diameter microneedle electrode penetrates the brain tissue *via* dissolvable material-based detachment and remains on it without being fixed to the cranium, resulting in a floating electrode architecture. Although the electrode device requires further advancements such as miniaturization and wireless recording system, the proposed recording technology showed clear advantages in terms of the high SNR during implantation and less tissue damage. These findings show that the proposed method will enable stable and safe chronic recording not only in the mice demonstrated in this study but also in other animals, including rats and monkeys.

Author contributions

K. Y., H. S., and T. K. designed the research. S. Ya. And K. Y. prepared the devices. K. Y. conducted the surgical procedure, animal experiment, and immunohistochemical experiment. K. Y., R. N., K. K., and T. K. analyzed the data. S. Yo. helped in the immunohistochemical experiment. K. Y. and T. K. wrote the manuscript. T. K. supervised the project.

Conflicts of interest

There are no conflicts to declare.

Acknowledgements

Notes and references

1 P. J. Rousche and R. A. Normann, *J. Neurosci. Methods*, 1998, **82**, 1–15.

2 Q. Bai, K. D. Wise and D. J. Anderson, *IEEE Trans. Biomed. Eng.*, 2000, **47**, 281–289.

3 J. J. Jun, N. A. Steinmetz, J. H. Siegle, D. J. Denman, M. Bauza, B. Barbarits, A. K. Lee, C. A. Anastassiou, A. Andrei, Ç. Aydin, M. Barbic, T. J. Blanche, V. Bonin, J. Couto, B. Dutta, S. L. Gratiy, D. A. Gutnisky, M. Häusser, B. Karsh, P. Ledochowitsch, C. M. Lopez, C. Mitelut, S. Musa, M. Okun, M. Pachitariu, J. Putzeys, P. D. Rich, C. Rossant, W. L. Sun, K. Svoboda, M. Carandini, K. D. Harris, C. Koch, J. O'Keefe and T. D. Harris, *Nature*, 2017, **551**, 232–236.

4 A. Obaid, M.-E. Hanna, Y.-W. Wu, M. Kollo, R. Racz, M. R. Angle, J. Müller, N. Brackbill, W. Wray and F. Franke, *Sci. Adv.*, 2020, **6**, eaay2789.

5 S. Takeuchi, T. Suzuki, K. Mabuchi and H. Fujita, *J. Micromech. Microeng.*, 2003, **14**, 104.

6 T. il Kim, J. G. McCall, Y. H. Jung, X. Huang, E. R. Siuda, Y. Li, J. Song, Y. M. Song, H. A. Pao, R. H. Kim, C. Lu, S. D. Lee, I. S. Song, G. Shin, R. Al-Hasani, S. Kim, M. P. Tan, Y. Huang, F. G. Omenetto, J. A. Rogers and M. R. Bruchas, *Science*, 2013, **340**, 211–216.

7 B. J. Kim, J. T. W. Kuo, S. A. Hara, C. D. Lee, L. Yu, C. A. Gutierrez, T. Q. Hoang, V. Pikov and E. Meng, *J. Neural Eng.*, 2013, **10**, 045002.

8 L. Luan, X. Wei, Z. Zhao, J. J. Siegel, O. Potnis, C. A. Tuppen, S. Lin, S. Kazmi, R. A. Fowler, S. Holloway, A. K. Dunn, R. A. Chitwood and C. Xie, *Sci. Adv.*, 2017, **3**, 1–10.

9 E. Musk, *J. Med. Internet Res.*, 2019, **21**, e16194.

10 K. Yamashita, H. Sawahata, S. Yamagiwa, Y. Morikawa, R. Numano, K. Koida and T. Kawano, *Sens. Actuators, B*, 2020, **316**, 127835.

11 R. Biran, D. C. Martin and P. A. Tresco, *Exp. Neurol.*, 2005, **195**, 115–126.

12 V. S. Polikov, P. A. Tresco and W. M. Reichert, *J. Neurosci. Methods*, 2005, **148**, 1–18.

13 H. Szarowski, D. Andersen, S. Retterer, J. Spence, M. Isaacson, G. Craighead, N. Turner and W. Shain, *Brain Res.*, 2003, **983**, 23–35.

14 R. Chen, A. Canales and P. Anikeeva, *Nat. Rev. Mater.*, 2017, **2**, 1–16.

15 S. M. Wellman, K. Guzman, K. C. Stieger, L. E. Brink, S. Sridhar, M. T. Dubaniewicz, L. Li, F. Cambi and T. D. Y. Kozai, *Biomaterials*, 2020, **239**, 119842.

16 T. D. Y. Kozai, X. Li, L. M. Bodily, E. M. Caparosa, G. A. Zenonos, D. L. Carlisle, R. M. Friedlander and X. T. Cui, *Biomaterials*, 2014, **35**, 9620–9634.

17 A. Hai, J. Shappir and M. E. Spira, *Nat. Methods*, 2010, **7**, 200–202.

18 L. Grob, H. Yamamoto, S. Zips, P. Rinklin, A. Hirano-Iwata and B. Wolfrum, *Adv. Mater. Technol.*, 2020, **5**, 1900517.

19 T. D. Y. Kozai, N. B. Langhals, P. R. Patel, X. Deng, H. Zhang, K. L. Smith, J. Lahann, N. A. Kotov and D. R. Kipke, *Nat. Mater.*, 2012, **11**, 1065.

20 H. Sawahata, S. Yamagiwa, A. Moriya, T. Dong, H. Oi, Y. Ando, R. Numano, M. Ishida, K. Koida and T. Kawano, *Sci. Rep.*, 2016, **6**, 35806.

21 A. Fujishiro, H. Kaneko, T. Kawashima, M. Ishida and T. Kawano, *Sci. Rep.*, 2014, **4**, 1–9.

22 Y. Kubota, S. Yamagiwa, H. Sawahata and S. Idogawa, *Sens. Actuators, B*, 2018, **258**, 1287–1294.

23 D. Seo, R. M. Neely, K. Shen, U. Singhal, E. Alon, J. M. Rabaey, J. M. Carmena and M. M. Maharbiz, *Neuron*, 2016, **91**, 529–539.

24 B. C. Johnson, K. Shen, D. Piech, M. M. Ghanbari, K. Y. Li, R. Neely, J. M. Carmena, M. M. Maharbiz and R. Muller, in *2018 IEEE Custom Integrated Circuits Conference (CICC)*, IEEE, 2018, pp. 1–4.

25 S. Yamagiwa, H. Sawahata, H. Oi, R. Numano, M. Ishida, K. Koida and T. Kawano, in *2017 IEEE 30th International Conference on Micro Electro Mechanical Systems (MEMS)*, IEEE, 2017, pp. 553–556.

26 A. Ikedo, T. Kawashima, T. Kawano and M. Ishida, *Appl. Phys. Lett.*, 2009, **95**, 33502.

27 K. Yamashita, H. Sawahata, S. Yamagiwa, R. Numano, K. Koida and T. Kawano, in *2019 20th International Conference on Solid-State Sensors, Actuators and Microsystems & Eurosensors XXXIII (TRANSDUCERS & EUROSENSORS XXXIII)*, IEEE, 2019, pp. 302–305.

28 H. Oka, K. Shimono, R. Ogawa, H. Sugihara and M. Taketani, *J. Neurosci. Methods*, 1999, **93**, 61–67.

29 K. Funayama, N. Hagura, H. Ban and Y. Ikegaya, *J. Neurosci.*, 2016, **36**, 11727–11738.

30 A. Lecomte, V. Castagnola, E. Descamps, L. Dahan, M. C. Blatché, T. M. Dinis, E. Leclerc, C. Egles and C. Bergaud, *J. Micromech. Microeng.*, 2015, **25**, 125003.

31 J. C. Barrese, N. Rao, K. Paroo, C. Triebwasser, C. Vargas-Irwin, L. Franquemont and J. P. Donoghue, *J. Neural Eng.*, 2013, **10**, 066014.

32 G. Lind, C. E. Linsmeier and J. Schouenborg, *Sci. Rep.*, 2013, **3**, 1–7.

33 N. J. Michelson, A. L. Vazquez, J. R. Eles, J. W. Salatino, E. K. Purcell, J. J. Williams, X. T. Cui and T. D. Y. Kozai, *J. Neural Eng.*, 2018, **15**, 33001.

34 T. D. Y. Kozai, A. L. Vazquez, C. L. Weaver, S.-G. Kim and X. T. Cui, *J. Neural Eng.*, 2012, **9**, 66001.

35 S. Zhang, J. Boyd, K. Delaney and T. H. Murphy, *J. Neurosci.*, 2005, **25**, 5333–5338.

36 S. M. Wellman, L. Li, Y. Yaxiaer, I. McNamara and T. D. Y. Kozai, *Front. Neurosci.*, 2019, **13**, 493.

37 D. Fan, D. Rich, T. Holtzman, P. Ruther, J. W. Dalley, A. Lopez, M. A. Rossi, J. W. Barter, D. Salas-Meza and S. Herwik, *PLoS One*, 2011, **6**, e22033.

38 T. A. Szuts, V. Fadeyev, S. Kachiguine, A. Sher, M. V. Grivich, M. Agrochão, P. Hottowy, W. Dabrowski, E. V. Lubenov and A. G. Siapas, *Nat. Neurosci.*, 2011, **14**, 263–269.

39 A. Zhou, S. R. Santacruz, B. C. Johnson, G. Alexandrov, A. Moin, F. L. Burghardt, J. M. Rabaey, J. M. Carmena and R. Muller, *Nat. Biomed. Eng.*, 2019, **3**, 15–26.

40 M. H. Ghaed, G. Chen, R. Haque, M. Wieckowski, Y. Kim, G. Kim, Y. Lee, I. Lee, D. Fick and D. Kim, *IEEE Trans. Circuits Syst. I Regul. Pap.*, 2013, **60**, 3152–3162.

41 S. Idogawa, K. Yamashita, R. Sanda, R. Numano, K. Koida and T. Kawano, *Sens. Actuators, B*, 2021, **331**, 129423.